




Cite this: *Environ. Sci.: Nano*, 2019, 6, 1838

Heterogeneous conversion of SO₂ on nano α -Fe₂O₃: the effects of morphology, light illumination and relative humidity†

Kejian Li,^a Lingdong Kong,^{*ab} Assiya Zhanzakova,^a Songying Tong,^a Jiandong Shen,^c Tao Wang,^a Lu Chen,^a Qing Li,^a Hongbo Fu^a and Liwu Zhang ^{*ad}

Hematite is one of the most important components in atmospheric mineral aerosols, which always presents different morphologies due to its different formation processes and various sources. However, less attention has been paid to the influences of the particle morphologies on atmospheric heterogeneous reactions as well as the contributions from illumination and moisture. In the present study, the impacts of these factors on the heterogeneous conversion of SO₂ on nano α -Fe₂O₃ particles with different morphologies were investigated in detail using *in situ* diffuse-reflectance infrared Fourier transform spectroscopy (DRIFTS). The results indicated that the heterogeneous reactivities were significantly different among four α -Fe₂O₃ samples with various shapes. Compared to the nanocapsule-like and hollow nanoring-like α -Fe₂O₃, hexagonal nanoplate-like and agglomerated nanoparticle-like α -Fe₂O₃ exhibited significantly greater uptake capacity of SO₂ probably due to the abundant reactive sites and larger BET surface area and pore size. In addition, light illumination enhanced the heterogeneous conversion of SO₂ on the four nano α -Fe₂O₃ samples; this might be due to the semiconducting property of hematite and comparatively low light intensity. Furthermore, moisture promoted the heterogeneous uptake of SO₂ on hexagonal nanoplate-like α -Fe₂O₃ in appropriate range; however, excess moisture was unfavorable for sulfate formation. Possible mechanisms were proposed in the present study. This study would be helpful in understanding the atmospheric heterogeneous processes and provides useful parameters for atmospheric modelling studies.

Received 23rd January 2019,
Accepted 11th April 2019

DOI: 10.1039/c9en00097f

rsc.li/es-nano

Environmental significance

Mineral aerosols have great impacts on the global climate and human health directly and indirectly, and the heterogeneous conversion of gaseous pollutants in the atmosphere plays an important role in aerosol formation. Numerous studies have been performed that have mainly focused on the impacts of moisture, temperature, and the composition of particles on this heterogeneous conversion. However, mineral dusts present different morphologies in the atmosphere due to their different formation processes and various sources. This study investigates, for the first time, the impact of morphology on the heterogeneous conversion of SO₂ on nano α -Fe₂O₃. We found that the uptake capacity was significantly different among four α -Fe₂O₃ with different shapes, probably due to their different BET specific surface areas, surface active sites, and crystal planes. In addition, the results indicated that light illumination enhanced the heterogeneous conversion and moisture promoted it in an appropriate range. This study makes up for the deficiencies in previous studies, and provides new insights for research into the atmospheric heterogeneous reactions.

1. Introduction

SO₂, mainly emitted from the combustion of fossil fuels, is a notorious gaseous pollutant in the atmosphere for forming acid rain and sulfate aerosols. Atmospheric chemistry studies have suggested that about half of the globally emitted SO₂ is converted to sulfate.^{1,2} The oxidation of SO₂ to sulfate in the atmosphere usually occurs *via* three pathways: gas phase oxidation by hydroxyl groups; aqueous phase oxidation in cloud or fog droplets by dissolved ozone, hydrogen peroxide and transition metal ions; and heterogeneous oxidation on the

^a Shanghai Key Laboratory of Atmospheric Particle Pollution and Prevention, Department of Environmental Science & Engineering, Fudan University, Shanghai, 200433, People's Republic of China. E-mail: ldkong@fudan.edu.cn, zhanglw@fudan.edu.cn

^b Shanghai Institute of Eco-Chongming (SIEC), No. 3663 Northern Zhongshan Road, Shanghai 200062, People's Republic of China

^c Hangzhou Environmental Monitoring Center, Hangzhou, People's Republic of China

^d Shanghai Institute of Pollution Control and Ecological Security, Shanghai, 200092, People's Republic of China

† Electronic supplementary information (ESI) available. See DOI: 10.1039/c9en00097f

surfaces of dust particles.^{3–5} Moreover, atmospheric chemistry models have been applied to explore the formation process and concentration of sulfate.^{6–8} The modeling simulations have indicated that the concentration of sulfate is usually underestimated, whereas the SO₂ concentration is overestimated as compared to the case of field measurements. On the other hand, sulfate formed from the gas phase and aqueous phase oxidation could not bridge the gap between field measurements and modeling simulations on a global scale.^{6,9,10} In addition, *via* field measurements, it has been found that the surfaces of atmospheric particles are usually coated with sulfate.¹¹ Therefore, the heterogeneous oxidation of SO₂ on the surfaces of atmospheric particles might play an important role in sulfate formation. Moreover, the heterogeneous conversion of SO₂ and the formation of sulfate will change the size, composition, and morphology of aerosol particles and thus have significant impacts on hygroscopicity, optical property and cloud condensation nuclei activity.¹² Many studies have been conducted to investigate the atmospheric heterogeneous conversion of SO₂ and other gases on the surface of nanoparticles. These studies are often focused on understanding the effects of relative humidity,^{13–15} temperature,^{11,16} the composition of nanoparticles,^{17,18} other gases such as O₃, NH₃, and NO₂,^{19–21} the crystal structure,^{14,22} and so on. However, there are still too many uncertainties in the complicated atmospheric heterogeneous reactions.

Mineral dust, emitted from arid and semi-arid regions, is a major component in the atmosphere. The annual flux of mineral dusts entering into the atmosphere is estimated to be about 1000–3000 Tg, which accounts for about 30–60% of global aerosols.^{23,24} Among these mineral dusts, size-resolved particulate matters containing nanoparticles inevitably exist. These mineral nanoparticles can be transported over thousands of kilometers, all the while providing reactive surfaces for the heterogeneous conversions of atmospheric reactive gases. Iron is an important component of mineral dusts, in which it usually exists in the form of iron oxides and oxyhydroxides.²² Significantly, iron oxide nanostructures are widespread in environmental ecosystems, and some researchers have reported that hematite could be employed as an environmental indicator, because Fe₂O₃ is more thermodynamically stable than other iron oxides, such as magnetite and goethite, under ambient conditions and also as the morphologies of naturally formed hematite nanocrystals have large variations depending on thermodynamic and chemical conditions.^{25,26} In nature, the typical morphologies of Fe₂O₃ nanocrystals are rounded, rhombohedral, and plate-like; among these, rounded and rhombohedral morphologies are common in low-temperature environments.^{26,27} In addition, hematite nanoparticles are mostly formed from different precursors mainly through solid-state transformation processes,²⁷ therefore, the obtained hematite may inherit or show some differences as compared with the precursor's morphologies. For example, hematite nanoparticles would present irregular hexagonal morphologies if they were formed

from ferrihydrite by internal rearrangement and dehydration within the ferrihydrite aggregates;²⁸ whereas hematite nanoparticles formed by the dehydration of akaganeite and lepidocrocite would maintain the rod- or lath-like morphology of the precursors at high temperatures (<300–400 °C).²⁹ Moreover, Guo *et al.* constructed a morphology map of hematite nanocrystals over a range of environmental conditions using modeling simulations, and the results indicated that the equilibrium shape of hematite could be rhombohedral, rounded, hexagonal, cubic, spherical, and so on.²⁵ Overall, we can see that the hematite particles show obviously different morphologies in nature depending on their formation process and the environmental conditions. Furthermore, while being one of the typical oxide minerals, Fe₂O₃ contributes ~6% by mass to the total mineral dusts burden in the atmosphere.³⁰ Therefore, it is reasonable that hematite would show different shapes in the atmosphere as well. Although the atmospheric chemical processes of Fe-containing dust particles during long-range transport can influence the levels of atmospheric gaseous pollutants, such as SO₂ and NO₂, the roles of the morphology of hematite in atmospheric heterogeneous reactions remain unclear. In addition, α -Fe₂O₃ is often used as a photocatalyst in wastewater treatment and water splitting due to its semiconducting property. Because the performances are always dependent on the morphology and size of the photocatalysts, researchers have paid much attention to prepare α -Fe₂O₃ with different morphologies and sizes with an aim to improve their performance.^{31–36} Furthermore, α -Fe₂O₃ is an important ingredient in steel manufacturing. Inevitably, the use of a large amount of α -Fe₂O₃ would make it enter into the atmosphere, where it will participate in atmospheric heterogeneous reactions. The different morphologies of mineral particles might then show different chemical reactivities, like cloud condensation nuclei activity. In the atmosphere, the particles usually are in a mixing state and thus it is complex and difficult to investigate the atmospheric heterogeneous reactions using multicomponent particles or sampled particles. Interestingly, previous studies suggested that single particle analyses could provide information about the mixing state of particles and explain the heterogeneous reactions occurring to a certain extent.^{37–39} A lot of researchers have tried to understand the mixing state of particles by analyzing a single particle through hygroscopicity, optical properties, heterogeneous reactivities as well as morphology.^{12,40,41} However, little attention has been paid to investigate the influence of morphology on the heterogeneous conversion of SO₂ and other reactive gases on atmospheric nanoparticles up to now.

Hence, in this study, we focused on the impact of the morphology of nano α -Fe₂O₃ on the heterogeneous conversion of SO₂, using *in situ* diffuse reflectance infrared Fourier transform spectroscopy (DRIFTS) and ion chromatography (IC). In addition, we also studied the effects of light illumination and relative humidity on the heterogeneous reactions. Four kinds of α -Fe₂O₃ with different morphologies were prepared and used as model nanoparticles. The results revealed that

α -Fe₂O₃ nanoparticles with different morphologies showed different uptake capacity. Light illumination improved the heterogeneous oxidation of SO₂ on α -Fe₂O₃ samples, while the relative humidity (RH) promoted SO₂ heterogeneous conversion in an appropriate range. This research provides a new insight for better understanding various influential factors involved in the heterogeneous formation of sulfate on mineral nanoparticles.

2. Experiments

2.1 Materials

All the chemicals were of analytical grade and used without further purification. Deionized water was used throughout the experiments (specific resistance ≥ 18.2 M Ω cm).

The methods utilized for the nano α -Fe₂O₃ samples synthesis are shown in the ESI.† The prepared four α -Fe₂O₃ samples with nanocapsule-like, hollow nanoring-like, hexagonal nanoplate-like, and aggregated nanoparticle-like morphologies (as discussed in section 3.1) were denoted as α -Fe₂O₃-A, α -Fe₂O₃-B, α -Fe₂O₃-C, and α -Fe₂O₃-D, respectively. The prepared samples were kept in a desiccator at 68% relative humidity (RH) for 24 h before the *in situ* DRIFTS experiments. The RH in the desiccator was controlled with a saturated solution of potassium iodide (Sigma-Aldrich). The samples were still loose powders after the treatment and some adsorbed water was present on the surfaces of the hematite samples.

In order to study the effect of the relative humidity on the heterogeneous conversion of SO₂ on α -Fe₂O₃, we chose α -Fe₂O₃-C as a typical sample. The sample was kept in a desiccator at 68% relative humidity for 0, 12, 24, 48, 72, and 96 h, respectively. These treated samples were denoted as 68% RH saturation time-0 h, -12 h, -24 h, -48 h, -72 h, and -96 h, respectively.

N₂ and O₂ (99.999% purity, Shanghai Yunguang Specialty Gases Inc.) were introduced through an air dryer of silica gel and a molecular sieve before use. SO₂ (100 ppm, SO₂/N₂, Shanghai Yunguang Specialty Gases Inc.) was used as a reactant gas in the experiments. A xenon lamp with a light intensity of about 15 mW cm⁻² was used as the light source to study the effect of light illumination.

2.2 Sample characterizations

The crystal structures of the as-prepared four α -Fe₂O₃ samples were characterized by powder X-ray diffraction (XRD, Bruker D8 Advance) using an X-ray diffractometer with Cu K α radiation ($\lambda = 1.54$ Å) ranging from 20° to 70° (2θ) with a scan speed of 2° min⁻¹. Micromorphology analysis of the four nano α -Fe₂O₃ samples was performed by field emission scanning electron microscopy (FE-SEM, Hitachi S-4800, Japan). The BET specific surface area and pore size of the samples were analyzed from nitrogen adsorption-desorption isotherms measured at 78 K on a Micromeritics Tristar 3000.

2.3 *In situ* DRIFTS experiments

In situ DRIFTS spectra were recorded using a Nicolet Avatar 360 FTIR spectrometer, equipped with a diffuse reflectance accessory and a high-sensitivity MCT detector cooled by liquid N₂. The reaction chamber and the sample were coupled with a temperature controller. The whole DRIFTS apparatus was similar to that used in previous studies.^{4,42}

First, 50 \pm 0.02 mg of the hematite sample was placed into a ceramic crucible in the reaction chamber, and the chamber and the sample were kept at 298 K by using a temperature controller. Before the reactant gas was introduced, the chamber and the sample were purged by a stream of synthetic air in a total flow rate of 100 mL min⁻¹ for 1 h, in order to remove the physically adsorbed water and impurities. Then, a single-beam spectrum was collected as the background spectrum. After that, a mixture of SO₂ (3%, v/v) and O₂ (21%, v/v) with N₂ as the carrier was introduced into the reaction chamber at a total flow rate of 100 mL min⁻¹. In order to study the effect of simulated light illumination on the heterogeneous conversion of SO₂, simulated solar irradiation was applied to the particles with a light intensity of ~ 15 mW cm⁻² supplied by a xenon lamp simultaneously.

The infrared spectra ranging from 4000 to 650 cm⁻¹ were collected automatically every 10 min until the total reaction time reached 2 h. The infrared spectra were recorded at a resolution of 4 cm⁻¹ with 100 scans for each spectrum. Every experiment was repeated at least two times.

2.4 Ion analysis

The generated surface products were analyzed using ion chromatography after the DRIFTS experiments. The reacted nanoparticles were extracted with 5 mL ultrapure water containing 5% formaldehyde to suppress sulfite/bisulfite oxidation.⁴ After ultrasonication for 5 min, the mixture was filtered through a 0.22 μ m PTFE membrane, and the obtained solution was analyzed using a Metrohm 883 Basic IC. A weak base eluent (1.0 mM NaHCO₃/3.5 mM Na₂CO₃) was used for anion detection at a flow rate of 1.5 mL min⁻¹. Quality assurance of the species measurement was carried out by consulting standard reference materials produced by the National Research Center for Certified Reference Materials, China.

3. Results and discussion

3.1 Characterizations of α -Fe₂O₃

The crystal structure of the as-prepared four samples were performed using a X-ray diffractometer as shown in Fig. 1. It was clear that all the diffraction peaks of the prepared samples matched well with the standard peaks of α -Fe₂O₃ (JCPDS 33-0664), with lattice constants of $a = 0.5013$ nm and $c = 1.3751$ nm.^{43,44} Moreover, the two main diffraction peaks at about 33.1° and 35.6° corresponded to the (104) and (110) planes, respectively. It could be observed that the (110) plane was stronger than the (104) plane in the α -Fe₂O₃-C sample, while the (104) plane was stronger than the (110) plane in

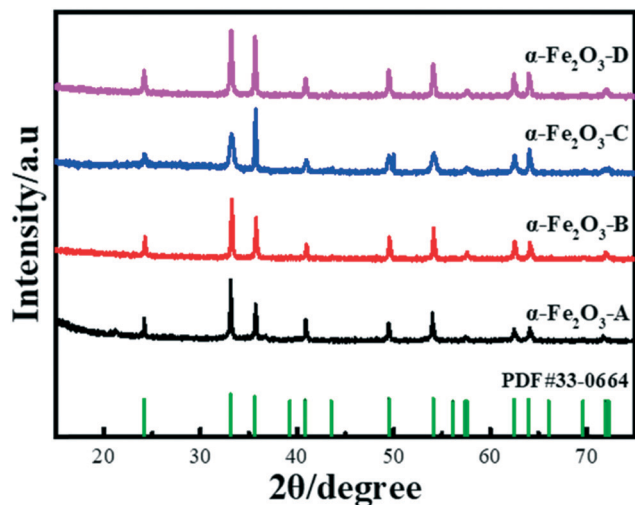


Fig. 1 XRD patterns of the four prepared α -Fe₂O₃ samples.

the other three samples. The different predominant crystal plane in the α -Fe₂O₃-C sample resulted from its uniform 2-dimensional (2D) hexagonal structure, namely, the (110) plane in the α -Fe₂O₃-C sample was the hexagonal face.⁴⁵ Moreover, there were no other peaks observed, indicating the prepared samples were α -Fe₂O₃ crystals with high purity. In

addition, the narrow and sharp peaks suggested that the prepared α -Fe₂O₃ samples had high-level crystallinity. Therefore, the XRD results verified that the four synthesized samples were pure α -Fe₂O₃ particles with high crystallinity.

A detailed investigation of the micromorphologies of the as-prepared four α -Fe₂O₃ samples was carried out, with Fig. 2 presenting the obtained FE-SEM images. It could be seen that α -Fe₂O₃-A (Fig. 2a) was mainly composed of uniform nanocapsule-like particles with an average particle size of about 900 nm \times 450 nm. The average size of α -Fe₂O₃-A was larger than 100 nm; therefore, theoretically, it does not belong to the nanoparticles class. However, its size was still very small so we named it as possessing nanocapsule-like particles in this study. The SEM image of α -Fe₂O₃-B (Fig. 2b) implied that it was composed of homogeneous hollow nanoring-like structures, with an average size of about 150 nm (outer and inner diameters of about 120 nm and 70 nm, respectively). The microstructure of α -Fe₂O₃-C (Fig. 2c) was a symmetrical hexagonal nanoplate-like, and the length of the diagonal was around 150 nm and the thickness was about 10 nm. Besides, the microstructure of α -Fe₂O₃-D (Fig. 2d) was composed of numerous nanoparticles with diameters of about 75 nm. Moreover, the size distribution of the four α -Fe₂O₃ samples was analyzed based on the SEM images, as

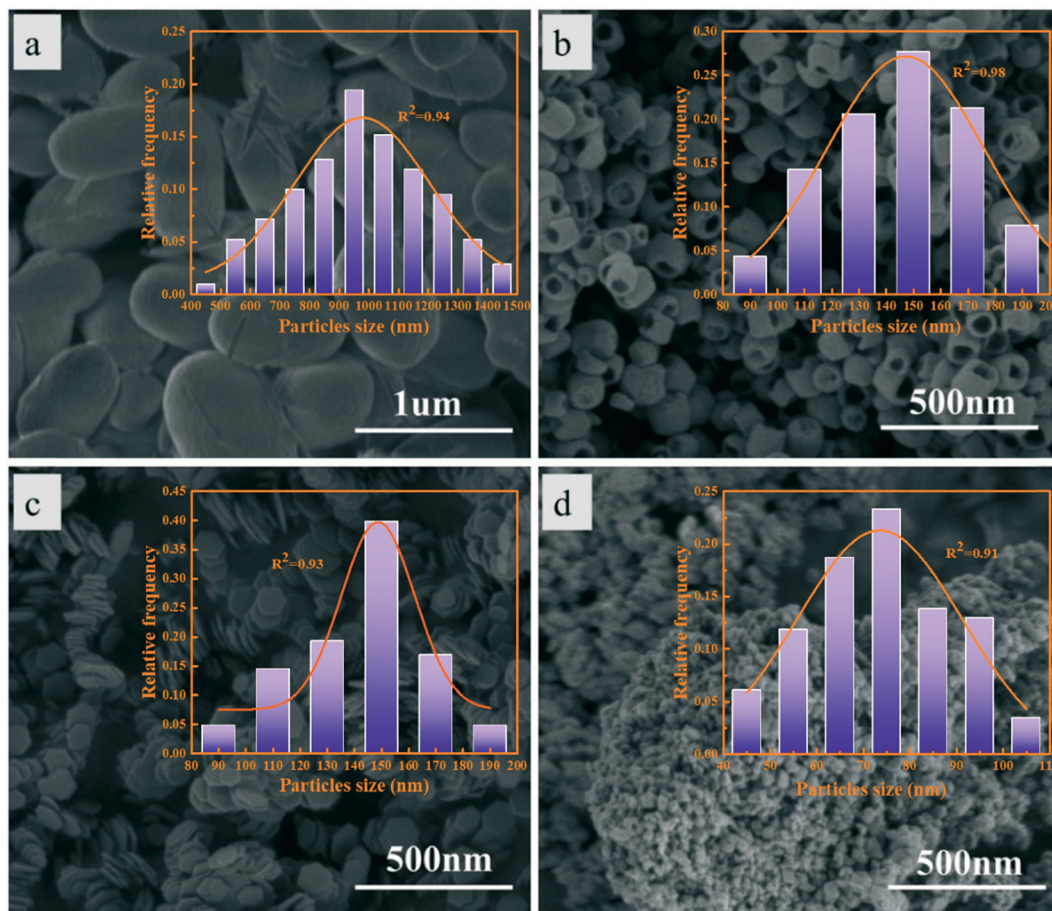


Fig. 2 SEM images and size distribution of the synthesized α -Fe₂O₃ samples: (a), α -Fe₂O₃-A. (b), α -Fe₂O₃-B. (c), α -Fe₂O₃-C, (d), α -Fe₂O₃-D.

shown in the inset in Fig. 2. It could be seen that the distribution curves fit the Gaussian function well with R^2 values of 0.94, 0.98, 0.93, and 0.91 for α -Fe₂O₃-A, α -Fe₂O₃-B, α -Fe₂O₃-C, and α -Fe₂O₃-D, indicating that the size distribution of the four samples was consistent with a normal distribution. It was clear that the four prepared α -Fe₂O₃ samples showed obviously different morphologies. Therefore, it would clearly be appropriate for us to investigate the effect of morphology on the atmospheric heterogeneous oxidation of SO₂.

Furthermore, the N₂ adsorption-desorption isotherms of the four samples are shown in Fig. 3. In Fig. 3, all the isotherms of the four α -Fe₂O₃ samples could be classified as type IV in the IUPAC classification with hysteresis loops in the relative pressure range of $0.8 < p/p^0 < 1.0$, suggesting the presence of large secondary mesoporous architectures (pore sizes are in the range of 2 to 50 nm). In addition, it was clear that the adsorption abilities were also different in the order of α -Fe₂O₃-D > α -Fe₂O₃-C > α -Fe₂O₃-B > α -Fe₂O₃-A, which is consistent with their specific surface areas (as shown in the inset in Fig. 3). On the other hand, the obtained pore size and pore volume of the four samples increased following the order: α -Fe₂O₃-B < α -Fe₂O₃-A < α -Fe₂O₃-C < α -Fe₂O₃-D. All the pore sizes were in the range of 10–20 nm, indicating the secondary mesoporous structures of the four α -Fe₂O₃ samples. It could be seen that the pore size of α -Fe₂O₃-B was smaller than that of α -Fe₂O₃-A, but α -Fe₂O₃-B showed a higher specific surface area than α -Fe₂O₃-A. This might result from the hollow nanoring-like microstructure, namely, there were outer and inner surfaces in the α -Fe₂O₃-B sample, which would increase its specific surface area. The relations between the results obtained from the N₂ adsorption-desorption isotherms and the heterogeneous reactivities are discussed later.

3.2 Effect of morphology on heterogeneous reactions

3.2.1. Surface sulfur-containing species and hydroxyl groups. In this section, *in situ* DRIFTS experiments were car-

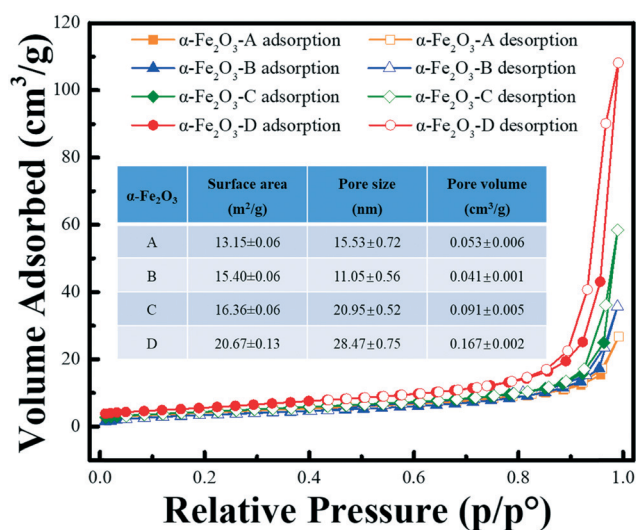


Fig. 3 N₂ adsorption-desorption isotherms and other parameters (inset) of the four α -Fe₂O₃ samples.

ried out at 298 K without light illumination to study the effect of the morphology of nano α -Fe₂O₃ on the heterogeneous uptake of SO₂.

DRIFTS spectra can provide valuable information of adsorbed surface species by the vibrational modes. According to previous studies,^{4,46–48} the peaks between 3700 cm⁻¹ and 3500 cm⁻¹ were ascribed to the vibrations of surface hydroxyl groups. The peak at about 1250 cm⁻¹ was attributed to free SO₄²⁻. The peak at around 1150 cm⁻¹ was assigned to adsorbed bidentate SO₄²⁻. Peaks at 1050 cm⁻¹ and 1010 cm⁻¹ were attributed to bridging SO₄^{2-/HSO}₄⁻. In addition, vibrational bands in the range of 1000–900 cm⁻¹ corresponded to chemisorbed SO₃^{2-/HSO}₃⁻. Fig. 4 shows the *in situ* DRIFTS spectra (1400–900 cm⁻¹) of the formed surface-bound species on the four samples as a function of time. It is clear that new vibrational bands could be observed after SO₂ exposure, and the intensities of these peaks increased with the time increasing. On the other hand, the DRIFTS spectra were distinct between α -Fe₂O₃ samples with different morphologies. Fig. 4a displays the DRIFTS spectra of surface species on nanocapsule-like α -Fe₂O₃ (α -Fe₂O₃-A) as the reaction proceeded. The main absorption peak at 1265 cm⁻¹ and weak peaks ranging from 1000–900 cm⁻¹ were observed, which could be attributed to free sulfate and sulfite/bisulfite, respectively. Besides, very weak bands between 1090–1000 cm⁻¹ assigned to other SO₄^{2-/HSO}₄⁻ also existed. The *in situ* DRIFTS spectra indicated that the prominent surface species were free sulfate after SO₂ was exposed on α -Fe₂O₃-A. The *in situ* DRIFTS spectra collected on the hollow nanoring-like α -Fe₂O₃ (α -Fe₂O₃-B) are shown in Fig. 4b. There are two peaks visible at about 1080 and 978 cm⁻¹, which were assigned to bridging sulfate/bisulfate and sulfite/bisulfite, respectively. Noticeably, the dominant generated surface species were bridging SO₄^{2-/HSO}₄⁻, which is different from the case of α -Fe₂O₃-A. Fig. 4c presents the vibrational bands recorded on the hexagonal nanoplate-like sample (α -Fe₂O₃-C). Two prominent peaks at 1247 and 1156 cm⁻¹ and a weak shoulder peak at 1028 cm⁻¹ can be clearly observed in the spectra. These peaks should be ascribed to free SO₄²⁻, bidentate SO₄²⁻ and bridging SO₄^{2-/HSO}₄⁻ according to previous studies, respectively. Fig. 4d shows the spectra collected on the agglomerated nanoparticle-like sample (α -Fe₂O₃-D) with SO₂ exposure. There are two prominent peaks at 1244 cm⁻¹ and 1159 cm⁻¹, which were attributed to free SO₄²⁻ and bidentate SO₄²⁻, respectively. Moreover, two shoulder peaks at 1056 and 1012 cm⁻¹ can be observed, which could be assigned to bridging sulfate/bisulfate. Similar to the α -Fe₂O₃-C sample, less SO₃^{2-/HSO}₃⁻ species were detected on the surface of α -Fe₂O₃-D. In addition, compared to the strong peaks of the formed sulfates on α -Fe₂O₃-C and α -Fe₂O₃-D, signals of the formed species on α -Fe₂O₃-A and α -Fe₂O₃-B were very low, indicating nanocapsule-like and hollow nanoring-like α -Fe₂O₃ particles were unfavorable for the heterogeneous oxidation of SO₂. According to the above analyses, we could find that the formed surface species during heterogeneous reactions included sulfate/bisulfate and sulfite/bisulfite. However, the

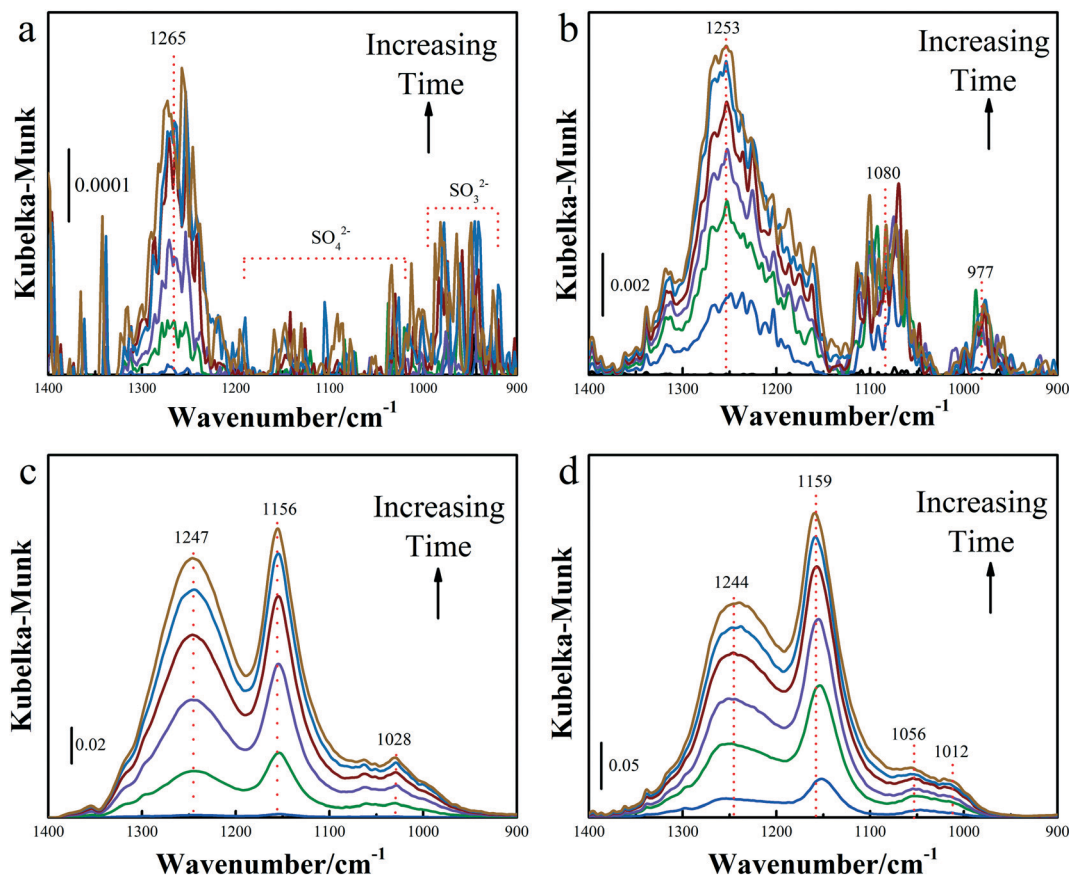


Fig. 4 *In situ* DRIFTS spectra collected on the four different samples (1400–900 cm^{-1}): (a), $\alpha\text{-Fe}_2\text{O}_3\text{-A}$. (b), $\alpha\text{-Fe}_2\text{O}_3\text{-B}$. (c), $\alpha\text{-Fe}_2\text{O}_3\text{-C}$, (d), $\alpha\text{-Fe}_2\text{O}_3\text{-D}$.

four $\alpha\text{-Fe}_2\text{O}_3$ samples showed different dominant surface species and the intensity of these vibrational bands was also significantly different. In other words, the shape evolution of mineral dusts influences their heterogeneous reactivities and the generated species.

With the help of surface reactive hydroxyl groups and other surface active sites, gaseous SO_2 could form chemisorbed sulfite or be further oxidized to sulfate species on the surfaces of nanoparticles. Therefore, we also discuss the variation of surface hydroxyl groups on the surface of the nanoparticles as the reaction proceeded. Fig. 5 displays the *in situ* DRIFTS spectra ($3720\text{--}3550\text{ cm}^{-1}$) collected on the four $\alpha\text{-Fe}_2\text{O}_3$ samples without light illumination. On the nanocapsule-like and nanoring-like $\alpha\text{-Fe}_2\text{O}_3$ particles (Fig. 5a and b), many negative peaks assigned to surface hydroxyl groups were observed, and their intensities increased with the time increasing, implying their consumption as the reaction proceeded. However, it should be noted that this consumption was very low as compared to those seen in Fig. 5c and d, which is consistent with the comparatively low heterogeneous reactivities of the two samples. On the hexagonal nanoplate-like sample (Fig. 5c), one prominent negative peak at 3622 cm^{-1} and two negative shoulder peaks at 3632 and 3612 cm^{-1} were observed. These peaks were also ascribed

to surface hydroxyl groups, and the fewer types of reactive hydroxyl groups on its surface may be attributed to its regular hexagonal shape. On the agglomerated nanoparticle-like sample (Fig. 5d), four negative peaks at 3666 , 3653 , 3635 , and 3621 cm^{-1} were observed, which were attributed to surface hydroxyl groups bonded to the surface iron species of octahedral sites and tetrahedral sites.^{4,22} The intensities of these negative peaks increased with the time increasing, implying that surface hydroxyl groups were consumed in the heterogeneous reactions.^{22,49} Therefore, the results reflected the different distributions and reactivities of the hydroxyl groups on the surfaces of $\alpha\text{-Fe}_2\text{O}_3$ with different morphologies, which might be responsible for the different uptake capacity to a certain extent.

3.2.2. Quantitative analysis and uptake coefficient. It has been reported that the concentration of generated surface species has a positive linear relationship with the integrated absorbance based on DRIFTS spectra.^{4,9} Therefore, the ions of the surface sulfates species, including free sulfate, bidentate sulfate, bridging sulfate, and bisulfate, on the different $\alpha\text{-Fe}_2\text{O}_3$ samples were analyzed according to their integrated characteristic absorbance. A calibration curve of sulfates ions *versus* the integrated absorbance was obtained from IC analyses of a series of *in situ* DRIFTS experiments

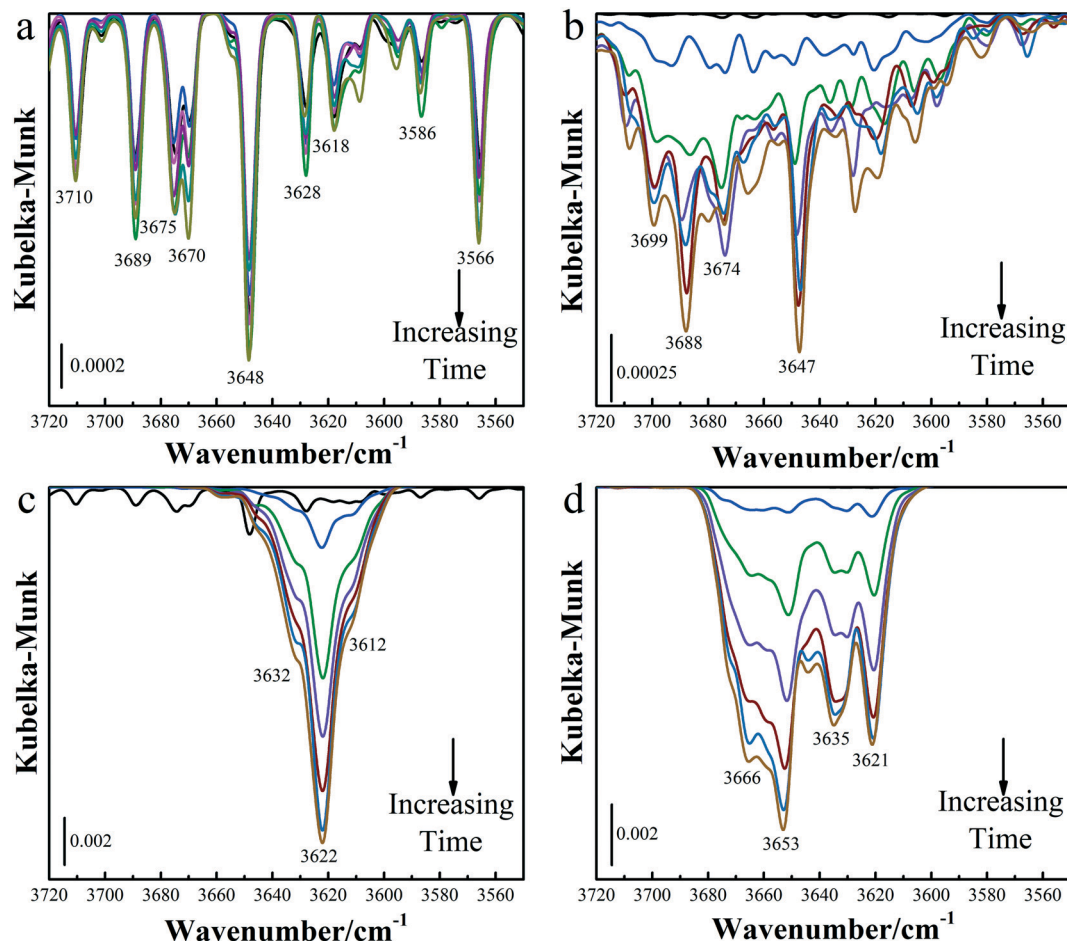


Fig. 5 *In situ* DRIFTS spectra collected on the four different α -Fe₂O₃ samples (3720–3550 cm⁻¹) without light illumination: (a), α -Fe₂O₃-A. (b), α -Fe₂O₃-B. (c), α -Fe₂O₃-C, (d), α -Fe₂O₃-D.

with different reaction times. The obtained value for the conversion factor was $f = 2.58 \times 10^{18}$ ions per g ABU (ABU, absorbance unit). In the present study, the ions of the generated sulfates species were calculated according to the formula expressed below:¹⁵

$$[\text{SO}_4^{2-}] = (\text{integrated absorbance}) \times f \quad (1)$$

Fig. 6 displays the calculated ions of the sulfates on different samples as a function of time under dark conditions. The slope of the curve could simply indicate the formation rates of sulfates species, and thus Fig. 6 also implied that the formation rates of sulfates first increased (initial stage) and then kept stable or decreased (stable stage) as the reaction proceeded. This was mainly because more surface reactive sites existed in the initial stage of SO₂ adsorption and oxidation. As the reaction proceeded, the number of active sites then decreased as generated species were adsorbed on them, which inhibited further SO₂ adsorption.^{13,22} Moreover, it was evident that the ions of the sulfates species generated on the different α -Fe₂O₃ samples were obviously different. The total ions of sulfates species decreased following the order: α -Fe₂O₃-D > α -Fe₂O₃-C > α -Fe₂O₃-B > α -Fe₂O₃-A. Interest-

ingly, this variation trend was opposite to the change in particle size and BET specific surface area as aforementioned. In other words, the smaller particles showed a larger surface

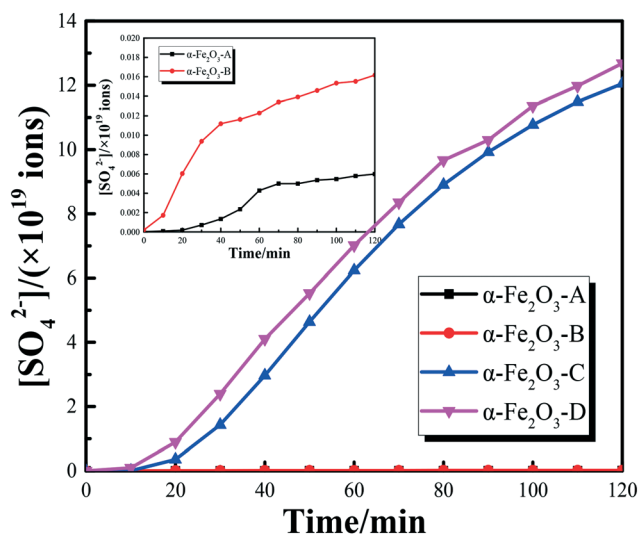


Fig. 6 Calculated ions of the sulfates on the different α -Fe₂O₃ samples without light illumination.

area and more active sites. The ions of the sulfates on α -Fe₂O₃-D were about 2500, 784, and 1.05 times greater as compared to on α -Fe₂O₃-A, α -Fe₂O₃-B, and α -Fe₂O₃-C. The α -Fe₂O₃-A sample presented the lowest heterogeneous reactivity, probably because its size (900 nm × 450 nm) was too large to supply efficient active sites for SO₂ adsorption and conversion. Therefore, the results of this study indicated that the particle size is also a factor in the heterogeneous reactions. Importantly, the BET specific surface area of α -Fe₂O₃-C (16.35 ± 0.06 m² g⁻¹) was closer to that of α -Fe₂O₃-B (15.40 ± 0.04 m² g⁻¹) and much less than that of α -Fe₂O₃-D (20.67 ± 0.13 m² g⁻¹), but the reactivity of α -Fe₂O₃-C was closer to that of α -Fe₂O₃-D and much higher than that of α -Fe₂O₃-B. This result implied that the particle shape is a more significant impact factor for the heterogeneous conversion of SO₂. Therefore, the particles morphology would inevitably affect the atmospheric heterogeneous reactions, which should thus be paid more attention in further studies.

In order to further discuss the reasons for the different reactivities impacted by morphology, we also calculated the uptake coefficients of SO₂ on the different α -Fe₂O₃ samples. The uptake coefficient γ is defined as the number of reactive collisions between reactant gas molecules and the particle surface per unit time ($-d[\text{SO}_2]/dt$) divided by the total number of surface collisions per unit time (Z). The heterogeneous reaction on the surface of Fe₂O₃ was most likely irreversible because the products (SO₄²⁻/HSO₄⁻ and SO₃²⁻/HSO₃⁻) were in the solid phase and the reactants (SO₂ and O₂) were gaseous. The concentration of O₂ could be considered to be kept constant because it was very abundant as compared with SO₂. In addition, the concentration of active sites on α -Fe₂O₃ at the initial stage was constant with respect to SO₂. Moreover, previous studies have found that the correlation coefficients of $\ln[C/C_0]$ versus time (t) (where C_0 is the initial concentration of SO₂ and C is the concentration of SO₂) for metal oxides under different initial concentrations of SO₂ were greater than 0.95.^{4,17,22} Therefore, the heterogeneous oxidation of SO₂ was consistent with pseudo-first-order reaction kinetics, namely, $-d[\text{SO}_2]/dt = d[\text{SO}_4^{2-}]/dt = KC_{\text{SO}_2}$, where K is the rate constant and C_{SO_2} is the concentration of SO₂ at certain reaction times. The equations used for the uptake coefficients calculation based on pseudo-first-order kinetics are shown as the following;^{22,47}

$$\gamma_{\text{geo}} = \frac{d[\text{SO}_4^{2-}]/dt}{Z} \quad (2)$$

$$Z = \frac{1}{4} A_{\text{geo}} C_{\text{SO}_2} v_{\text{SO}_2} \quad (3)$$

$$v_{\text{SO}_2} = \sqrt{\frac{8RT}{\pi M_{\text{SO}_2}}} \quad (4)$$

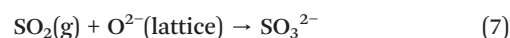
$$\gamma_{\text{BET}} = A_{\text{geo}} \times \gamma_{\text{geo}} / A_{\text{BET}} \quad (5)$$

where, γ_{geo} represents the geometric uptake coefficient, γ_{BET} is the BET uptake coefficient, $d[\text{SO}_4^{2-}]/dt$ represents the formation rate of sulfates (ion per s), v_{SO_2} is the mean molecular velocity of SO₂ (m s⁻¹), A_{geo} is the particle geometric surface area (m²), C_{SO_2} is the concentration of SO₂ (molecule per m³), R is the gas constant (J mol⁻¹ K⁻¹), T is the temperature (K), M_{SO_2} is the molecular weight of SO₂ (Kg mol⁻¹), and A_{BET} is the BET specific surface area (m² g⁻¹). Detailed information of these parameters is given in Table S1.† The upper and lower limits of the uptake coefficients are γ_{geo} and γ_{BET} dependent on the reaction probability, respectively.⁴

Table 1 presents the calculated uptake coefficients of SO₂ on the nano α -Fe₂O₃ samples at 298 K. Among the different samples, α -Fe₂O₃-D showed the highest amount of sulfates species, as shown in Fig. 6. Correspondingly, the aggregated nanoparticles-like α -Fe₂O₃ (α -Fe₂O₃-D) presented the highest γ_{geo} of $(1.32 \pm 0.09) \times 10^{-3}$. However, the BET uptake coefficients (γ_{BET}) did not follow the same order as the geometric uptake coefficients. The α -Fe₂O₃-C sample presented the highest γ_{BET} of $(2.05 \pm 0.12) \times 10^{-7}$, even though it did not show the highest ions of the produced sulfates species. This was probably because the hexagonal nanoplate-like α -Fe₂O₃-C had a smaller BET specific surface area than α -Fe₂O₃-D, while the ions of the sulfates species detected on α -Fe₂O₃-C (1.205×10^{20}) and α -Fe₂O₃-D (1.268×10^{20}) were similar. However, the γ_{geo} and γ_{BET} of α -Fe₂O₃-A and α -Fe₂O₃-B were lower by 3 orders of magnitude compared to the other two samples. Overall, it was clear that the uptake capacity of SO₂ was different among the four nanoscale α -Fe₂O₃ samples with different morphologies, probably because of the different BET surface areas, various pore sizes, different number of surface reactive sites, and so on.

3.2.3. Proposed mechanism. Even though the heterogeneous reactivities were obviously different between the α -Fe₂O₃ samples with different morphologies, the reaction mechanisms of SO₂ on the four α -Fe₂O₃ samples were almost similar due to the use of the same reactants, same experimental conditions, and similar products. The proposed mechanism is discussed below.

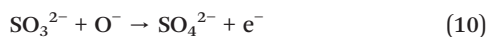
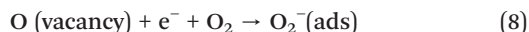
First, besides the reaction between SO₂ and adsorbed water to form S(IV) species,^{4,50} SO₂ is adsorbed on Lewis acid sites (coordinately unsaturated iron atoms) or Lewis basic sites (exposed oxygen atoms) to form physically adsorbed SO₂ or chemisorbed sulfite, respectively.^{11,51,52} The reactions are shown as eqn (6) and (7) below, where O²⁻ (lattice) means lattice oxygen on the surface of the particles.



The adsorbed oxygen form active oxygen *via* combining with an oxygen vacancy. Further, active oxygen oxidizes chemisorbed sulfite to sulfate.^{19,53,54} The reactions are as follows:

Table 1 Reactive surface areas and uptake coefficients of SO₂ on nano α-Fe₂O₃

| α-Fe ₂ O ₃ | Light | A _{BET} (m ² g ⁻¹) | A _{geo} (×10 ⁻⁵ m ²) | γ _{BET} | γ _{geo} |
|----------------------------------|---------|--|--|-----------------------------------|----------------------------------|
| A | Without | 13.15 ± 0.06 | 7.85 | (1.31 ± 0.13) × 10 ⁻¹⁰ | (6.60 ± 0.43) × 10 ⁻⁷ |
| | With | 13.15 ± 0.06 | 7.85 | (7.60 ± 0.67) × 10 ⁻¹⁰ | (3.82 ± 0.25) × 10 ⁻⁶ |
| B | Without | 15.40 ± 0.04 | 7.85 | (2.33 ± 0.11) × 10 ⁻¹⁰ | (1.37 ± 0.13) × 10 ⁻⁶ |
| | With | 15.40 ± 0.04 | 7.85 | (1.63 ± 0.13) × 10 ⁻⁹ | (9.58 ± 0.32) × 10 ⁻⁶ |
| C | Without | 16.35 ± 0.06 | 7.85 | (2.05 ± 0.12) × 10 ⁻⁷ | (1.28 ± 0.11) × 10 ⁻³ |
| | With | 16.35 ± 0.06 | 7.85 | (2.12 ± 0.14) × 10 ⁻⁷ | (1.32 ± 0.21) × 10 ⁻³ |
| D | Without | 20.67 ± 0.13 | 7.85 | (1.65 ± 0.12) × 10 ⁻⁷ | (1.32 ± 0.09) × 10 ⁻³ |
| | With | 20.67 ± 0.13 | 7.85 | (1.97 ± 0.11) × 10 ⁻⁷ | (1.56 ± 0.10) × 10 ⁻³ |



On the other hand, surface adsorbed hydroxyl groups would also be involved in the heterogeneous reactions. SO₂ reacts with hydroxyl groups to form chemisorbed bisulfite or sulfite, as shown in reactions (11) and (12). The consumption of hydroxyl groups has been discussed before (Fig. 5). Moreover, the generated sulfite or bisulfite would be oxidized by reactive oxygen, Fe(III)–Fe(II) redox cycling, and a series of radical reactions, like with SO₅^{·-}, HSO₅^{·-}, and SO₄^{·-}, to form sulfate or bisulfate.^{19,22,54}

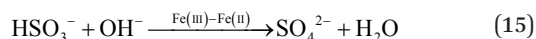
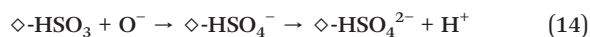
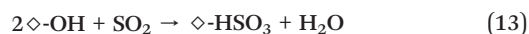
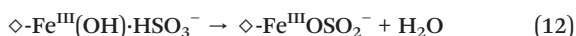
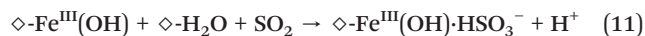


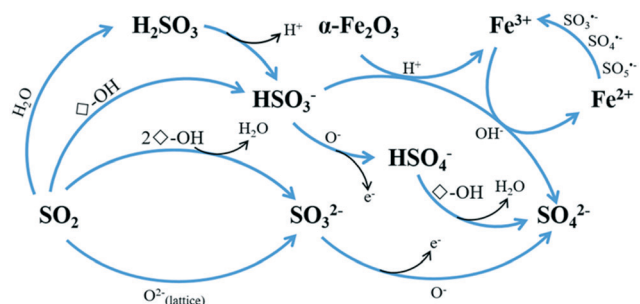
Fig. 7 shows the proposed mechanism for the heterogeneous reactions of SO₂ on hematite. Briefly, the surface adsorbed hydroxyl groups and active oxygen participate in the formation of sulfates species, and the existing Fe(III)–Fe(II) redox cycle also make contributions to the heterogeneous oxidation of SO₂. In this study, the results indicated that the heterogeneous reactivities were different between the four Fe₂O₃ samples with obviously different morphologies, suggesting the particles' morphology may be an important impact factor for the heterogeneous conversion of SO₂. The differences in the heterogeneous reactivities might result from differences in particle size, BET specific surface area, SO₂ adsorption ability, and number of surface active sites. In addition, different morphologies would provide different crystal planes, and different crystal planes would provide different surface active sites and their different distributions. The combined effect of these factors might lead to the differences in the heterogeneous reactivities of the various shapes. Further exploration and clarification are needed to explain

the reasons for the differences in heterogeneous reactivities among particles with different morphologies.

3.3 Effect of simulated light illumination on heterogeneous reactions

As there are complex physiochemical reactions in the atmosphere, solar light will inevitably influence these reactions. Nevertheless, simulation studies of heterogeneous reactions have to date always been carried out under dark conditions.^{14,22,55} In this study, we also investigated the effect of light illumination on the heterogeneous oxidation of SO₂ on the four α-Fe₂O₃ samples at 298 K with a light intensity of 15 mW cm⁻². Because the annual averaged light intensity reaching the mid-latitude region is about 100 mW cm⁻²,^{56,57} α-Fe₂O₃-D was first employed to study the effect of light illumination under a light intensity of 100 mW cm⁻². The results (data not shown) indicated that the heterogeneous conversion of SO₂ was inhibited under this condition, which might be due to the photoinduced reductive dissolution of α-Fe₂O₃ under stronger light intensity. Meanwhile, the light intensity was sometimes comparatively low, especially during severe haze episodes. Thus, in order to study whether there is a relation between a weak light intensity and severe haze events, we turned down the light intensity to about 15 mW cm⁻² to study the effect of light illumination in this study.

The collected *in situ* DRIFTS spectra (1400–900 cm⁻¹) under light illumination are shown in Fig. S1.† Brief analyses indicated the generated surface species included free sulfate, bidentate sulfate, bridging sulfate, and sulfite, which was similar to that collected without light illumination. There were negative bands in the DRIFTS spectra ranging from 3700 to 3550 cm⁻¹, which indicated the surface hydroxyl

**Fig. 7** The proposed mechanism in the present study.

groups were also consumed as the reactions proceeded under light illumination (as shown in Fig. S2†).

The DRIFTS spectra collected at 120 min with and without light illumination showed that the spectra were obviously different under the two experimental conditions (see Fig. 8). Under simulated light illumination, the dominant characteristic absorption peaks were almost similar as compared with those collected without light illumination except for α -Fe₂O₃-B. As for α -Fe₂O₃-B, the dominant characteristic absorption peak was at about 1258 cm⁻¹ under light illumination, while the main peak was at about 1080 cm⁻¹ under dark conditions. These results implied that light illumination indeed influenced the heterogeneous reactions and promoted the formation of sulfates. Importantly, the intensities of the DRIFTS spectra under light illumination were higher than those without light illumination for the four nano α -Fe₂O₃ samples. This result indicated that simulated light illumination improved the heterogeneous reactivities of the nano α -Fe₂O₃ samples with SO₂. Fig. S3† indicates that the formation rates of sulfates species could be classified into an initial stage and stable stage, which is consistent with the results obtained without light illumination and has been explained before. Furthermore, we compared the ions of the sulfates

measured under light illumination and without. As shown in Fig. 9, the amounts of sulfates under light illumination were higher than those without light illumination for all the α -Fe₂O₃ samples. The amounts of sulfates were about 7.23, 6.28, 1.03, and 1.07 times greater than those without illumination, respectively. Undoubtedly, γ_{geo} and γ_{BET} under light illumination were higher and the variation tendency of γ_{geo} and γ_{BET} was the same as that obtained without light illumination (as shown in Table 1). Therefore, the illumination promoted the heterogeneous oxidation of SO₂ on the four different nano α -Fe₂O₃ samples in this study.

Some previous studies found that UV light illumination inhibited the heterogeneous oxidation of SO₂ on hematite, and this phenomenon has often been explained by the photo-reduction of Fe₂O₃.⁵⁸ However, this study showed that light illumination enhanced the heterogeneous conversion of SO₂ on α -Fe₂O₃ nanoparticles under light illumination. The photoreduction of α -Fe₂O₃ was probably not dominant in the present study due to the lower light intensity and as there was less UV light in the light source (as shown in Fig. S4†). On another hand, α -Fe₂O₃, with a band gap of ~2.2 eV, is a promising semiconductor and is often used as a photocatalyst for water splitting and wastewater treatment. An

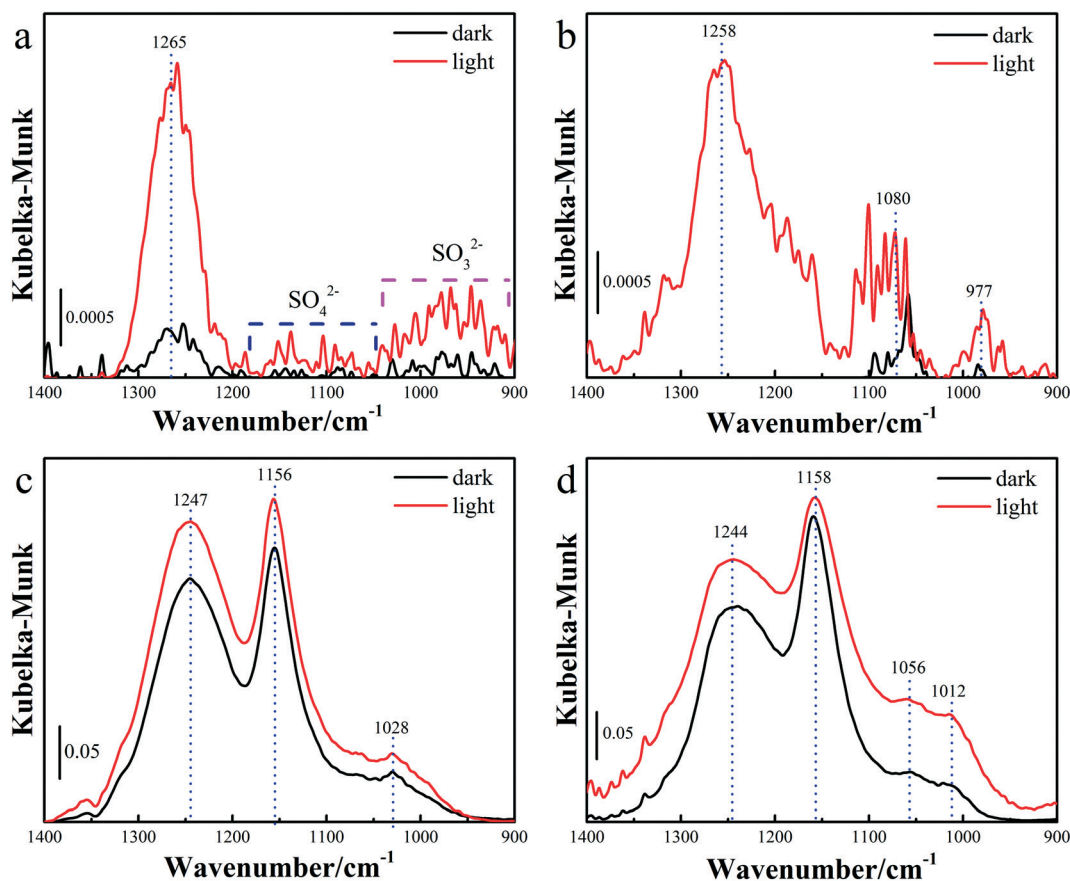


Fig. 8 *In situ* DRIFTS spectra obtained at 120 min with light illumination and without (1400–900 cm⁻¹): (a), α -Fe₂O₃-A, (b), α -Fe₂O₃-B, (c), α -Fe₂O₃-C, (d), α -Fe₂O₃-D.

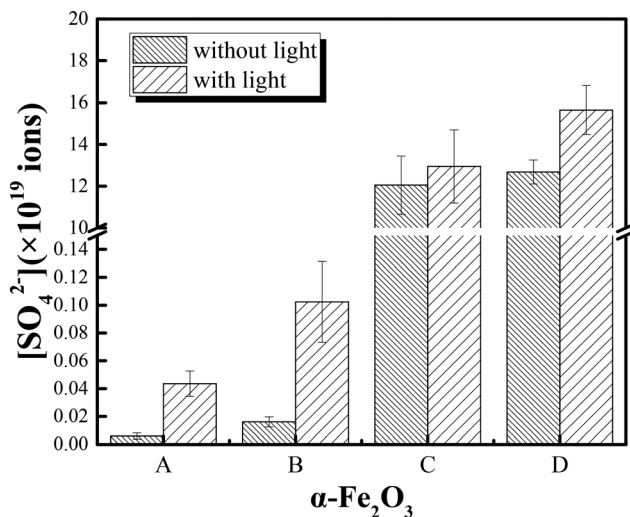
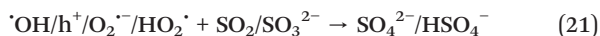
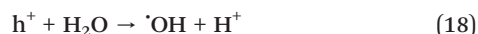
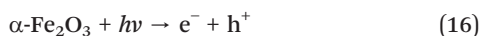


Fig. 9 Calculated sulfate ions in the absence and presence of illumination.

α -Fe₂O₃ semiconductor can generate electrons and holes under light illumination ($\lambda < 600$ nm), which would react with surface adsorbed H₂O and oxygen to produce \cdot OH, O₂^{•-}, and HO₂[•] radicals (as shown in eqn (16) to (21)).⁵⁹ These radicals have strong oxidation ability, and they can participate in heterogeneous oxidation of SO₂ and enhance sulfate formation.



Therefore, it was reasonable that the α -Fe₂O₃ samples exhibited semiconducting properties under light illumination to support the enhanced heterogeneous oxidation of SO₂ in the present study. In addition, a 300 W xenon lamp coupled with an optical fiber was used to supply simulated illumination, and emitted visible light with a light intensity of 15 mW cm⁻², and this relatively low light intensity might suppress the photoreduction of α -Fe₂O₃ to some extent. The light intensity and light source were different from those used in other studies, which might be another reason why the photoreduction of α -Fe₂O₃ was not observed in this study. Moreover, the results also simply indicated that a lower light intensity in severe haze episodes might be a reason for the severe haze events occurring. However, this study mainly focused on the effect of particle's morphology, therefore, we did not investigate the effect of light illumination under dif-

ferent light intensities and did not present a clearer relation between weak light intensity and haze events. In future, we will further study the effect of light illumination on heterogeneous reactions under different light intensities in detail. In addition, the proposed reaction mechanism in section 3.2.3 is also suitable under light illumination.

3.4 Effects of relative humidity on the heterogeneous reactions of SO₂ on α -Fe₂O₃-C

In the atmosphere, the relative humidity (RH) is a variable dependent on the temperature, altitude, and other factors. The varied RH would have effects on the atmospheric physiochemical processes. In order to clarify the effects of RH in this study, we chose α -Fe₂O₃-C as a typical sample for further investigations. The sample was kept in a desiccator at 68% RH for different times before the DRIFTS experiments, as described in section 2.1. The sample was not immersed in a solution after the equilibration, and hence heterogeneous aqueous reactions would not occur in our experiment. It was found that, on the samples treated by different saturation times at 68% RH, the *in situ* DRIFTS spectra (see Fig. S5†) were similar to each other except for their intensity. Three characteristic absorption peaks at about 1246, 1156, and 1027 cm⁻¹ were observed. The three peaks were attributed to surface adsorbed free sulfate, bidentate sulfate, and bridging sulfate/bisulfate species, respectively. The results implied that the varied relative humidity did not influence the generated surface species during the heterogeneous reactions. Apart from the similar spectra, it was clearly observed that the spectra intensities first increased and then decreased with increasing saturation time at 68% RH. Fig. 10 presents the obtained ions of the sulfates species on α -Fe₂O₃-C under different saturation times. The ions of the sulfates increased from 7.72×10^{19} ions to 1.33×10^{20} ions as the saturation time increased from 0 h to 48 h, and then decreased to 1.02×10^{20} when the saturation time was extended to 96 h. The results showed that the variation trend of ions was consistent with the intensities of the DRIFTS spectra. The experimental results implied that the heterogeneous conversion of SO₂ on α -Fe₂O₃-C was promoted by an appropriate amount of surface adsorbed water, while excess surface adsorbed water was unfavorable for the heterogeneous oxidation. The effect of the relative humidity on the heterogeneous reactivities of α -Fe₂O₃-C may also apply to other hematite samples.

In the present study, water was first adsorbed on the surface of α -Fe₂O₃-C, and then the reactant gases were adsorbed. Adsorbed water can react with Lewis acid sites on the sample surface to produce hydroxyl groups or can react with SO₂ directly to produce S(IV) species. Both would favor the oxidation of SO₂ as aforementioned. In addition, there existed compete adsorption between SO₂ and water molecules.^{13,14} At low relative humidity, there were still many exposed active sites for SO₂ adsorption and adsorbed water could re-produce hydroxyl groups to promote SO₂ oxidation. With the relative humidity increasing, the adsorbed water would occupy a larger

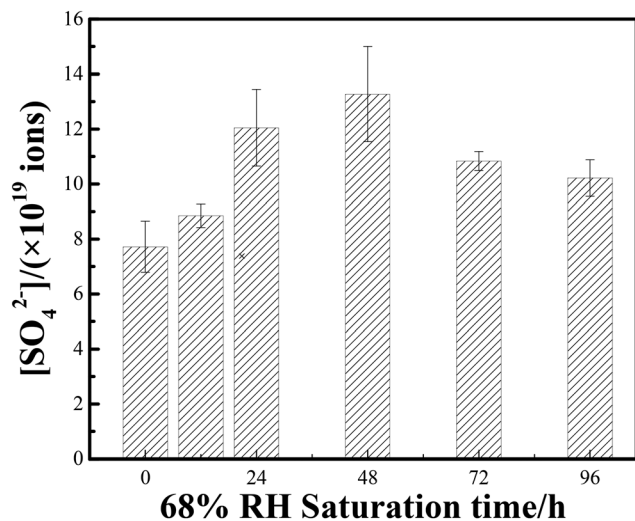


Fig. 10 Calculated ions of the sulfates on α -Fe₂O₃-C under different 68% RH saturation times.

number of the active sites. When RH saturation time was very long, the adsorbed water even would condense on the sample surface to form a water layer on the surface, which makes SO₂ need to pass through the water layer to reach the surface of the hematite. Consequently, SO₂ gas molecules could not be adsorbed on the hematite sample surface efficiently. This means that too much water adsorbed on the surface of α -Fe₂O₃-C would inhibit SO₂ uptake. A similar result was obtained in a previous study that focused on investigating the roles of the relative humidity on the heterogeneous reaction of SO₂ with soot.¹³ Therefore, the compete adsorption and liquid diffusion process totally suppressed the heterogeneous reactions.

4. Conclusion and atmospheric implications

In the present study, the effects of the morphology, light illumination, and relative humidity on the heterogeneous conversion of SO₂ on nano α -Fe₂O₃ were investigated in detail. The results indicated that nano α -Fe₂O₃ samples with various morphologies showed different reactivities, which might be due to the different specific surface areas and different surface reactive sites. Hexagonal nanoplate-like and agglomerated nanoparticle-like α -Fe₂O₃ showed higher heterogeneous reactivities, which might be due to their higher BET surface area and more abundant surface reactive sites. Simulated light illumination promoted the heterogeneous oxidation of SO₂ on α -Fe₂O₃ samples, which might be a result of their semiconducting properties and lower light intensity. In addition, appropriate moisture favored the heterogeneous conversion of SO₂, while excess relative humidity presented an inhibitory effect.

This study revealed the impacts of these three factors on the heterogeneous conversion of SO₂ on hematite, which have important atmospheric implications. The heterogeneous con-

version of SO₂ in the atmosphere would be affected by the shape evolution of mineral dusts. Therefore, care should be taken to the shape evolution of mineral dusts in field measurements and its influence on atmospheric chemistry. In addition, solar light will inevitably influence the atmospheric chemical reactions. The results indicated that the heterogeneous conversion of polluted gases on some dust particles might show different reactivities at daytime and nighttime. Moreover, atmospheric relative humidity also has complex effects on the heterogeneous conversion of SO₂ on mineral dust particles. All these factors should be studied deeply to help us further understand heterogeneous reactions, and thus to promote atmospheric chemistry research and modeling.

Conflicts of interest

The authors declare no competing financial interest.

Acknowledgements

This study was supported by the National Key R & D Program of China (2017YFC0209505) and the National Natural Science Foundation of China (Grant Nos. 21777027, 41475110, 21277028, and 21677037).

References

- J. W. Adams, D. Rodriguez and R. A. Cox, The uptake of SO₂ on Saharan dust: a flow tube study, *Atmos. Chem. Phys.*, 2005, 5, 2679–2689.
- Z. Levin, E. Ganor and V. Gladstein, The Effects of Desert Particles Coated with Sulfate on Rain Formation in the Eastern Mediterranean, *J. Appl. Meteorol.*, 1928, 35, 1511–1523.
- V. M. Kerminen, L. Pirjola, M. Boy, A. Eskola, K. Teinilä, L. Laakso, A. Asmi, J. Hienola, A. Lauri and V. Vainio, Interaction between SO₂ and submicron atmospheric particles, *Atmos. Res.*, 2000, 54, 41–57.
- L. D. Kong, X. Zhao, Z. Y. Sun, Y. W. Yang, H. B. Fu, S. C. Zhang, T. T. Cheng, X. Yang, L. Wang and J. M. Chen, The effects of nitrate on the heterogeneous uptake of sulfur dioxide on hematite, *Atmos. Chem. Phys.*, 2014, 14, 9451–9467.
- G. Wang, R. Zhang, M. E. Gomez, L. Yang, M. Levy Zamora, M. Hu, Y. Lin, J. Peng, S. Guo, J. Meng, J. Li, C. Cheng, T. Hu, Y. Ren, Y. Wang, J. Gao, J. Cao, Z. An, W. Zhou, G. Li, J. Wang, P. Tian, W. Marrero-Ortiz, J. Secret, Z. Du, J. Zheng, D. Shang, L. Zeng, M. Shao, W. Wang, Y. Huang, Y. Wang, Y. Zhu, Y. Li, J. Hu, B. Pan, L. Cai, Y. Cheng, Y. Ji, F. Zhang, D. Rosenfeld, P. S. Liss, R. A. Duce, C. E. Kolb and M. J. Molina, Persistent sulfate formation from London Fog to Chinese haze, *Proc. Natl. Acad. Sci. U. S. A.*, 2016, 113, 13630–13635.
- P. Kasibhatla, W. L. Chameides and J. StJohn, A three-dimensional global model investigation of seasonal variations in the atmospheric burden of anthropogenic sulfate aerosols, *J. Geophys. Res.: Atmos.*, 1997, 102, 3737–3759.

- 7 C. D. O'Dowd, J. A. Lowe, N. Clegg, M. H. Smith and S. L. Clegg, Modeling heterogeneous sulphate production in maritime stratiform clouds, *J. Geophys. Res.: Atmos.*, 2000, **105**, 7143–7160.
- 8 Z. Yu, M. Jang and J. Park, Modeling atmospheric mineral aerosol chemistry to predict heterogeneous photooxidation of SO₂, *Atmos. Chem. Phys.*, 2017, **17**, 1–34.
- 9 C. Liu, Q. X. Ma, Y. C. Liu, J. Z. Ma and H. He, Synergistic reaction between SO₂ and NO₂ on mineral oxides: a potential formation pathway of sulfate aerosol, *Phys. Chem. Chem. Phys.*, 2012, **14**, 1668–1676.
- 10 M. Luria and H. Sievering, Heterogeneous and homogeneous oxidation of SO₂ in the remote marine atmosphere, *Atmos. Environ., Part A*, 1991, **25**, 1489–1496.
- 11 L. Y. Wu, S. R. Tong, W. G. Wang and M. F. Ge, Effects of temperature on the heterogeneous oxidation of sulfur dioxide by ozone on calcium carbonate, *Atmos. Chem. Phys.*, 2011, **11**, 6593–6605.
- 12 M. B. Altaf, D. D. Dutcher, T. M. Raymond and M. A. Freedman, Effect of particle morphology on cloud condensation nuclei Activity, *ACS Earth Space Chem.*, 2018, **2**(6), 634–639.
- 13 Y. Zhao, Y. Liu, J. Ma, Q. Ma and H. He, Heterogeneous reaction of SO₂ with soot: The roles of relative humidity and surface composition of soot in surface sulfate formation, *Atmos. Environ.*, 2017, **152**, 465–476.
- 14 W. Yang, J. Zhang, Q. Ma, Y. Zhao, Y. Liu and H. He, Heterogeneous Reaction of SO₂ on Manganese Oxides: the Effect of Crystal Structure and Relative Humidity, *Sci. Rep.*, 2017, **7**, 4550.
- 15 Y. Zhang, S. Tong, M. Ge, B. Jing, S. Hou, F. Tan, Y. Chen, Y. Guo and L. Wu, The influence of relative humidity on the heterogeneous oxidation of sulfur dioxide by ozone on calcium carbonate particles, *Sci. Total Environ.*, 2018, **633**, 1253–1262.
- 16 H. X. Cui, T. T. Cheng, J. M. Chen, Y. F. Xu and W. Fang, A Simulated Heterogeneous Reaction of SO₂ on the Surface of Hematite at Different Temperatures, *Acta Phys.-Chim. Sin.*, 2008, **24**, 2331–2336.
- 17 X. Y. Zhang, G. S. Zhuang, J. M. Chen, Y. Wang, X. Wang, Z. S. An and P. Zhang, Heterogeneous reactions of sulfur dioxide on typical mineral particles, *J. Phys. Chem. B*, 2006, **110**, 12588–12596.
- 18 J. Y. Park and M. Jang, Heterogeneous photooxidation of sulfur dioxide in the presence of airborne mineral dust particles, *RSC Adv.*, 2016, **6**, 58617–58627.
- 19 W. Yang, H. He, Q. Ma, J. Ma, Y. Liu, P. Liu and Y. Mu, Synergistic formation of sulfate and ammonium resulting from reaction between SO₂ and NH₃ on typical mineral dust, *Phys. Chem. Chem. Phys.*, 2016, **18**, 956–964.
- 20 L. Wu, S. Tong, L. Zhou, W. Wang and M. Ge, Synergistic Effects between SO₂ and HCOOH on α -Fe₂O₃, *J. Phys. Chem. A*, 2013, **117**, 3972–3979.
- 21 Q. X. Ma, Y. C. Liu and H. He, Synergistic effect between NO₂ and SO₂ in their adsorption and reaction on gamma-alumina, *J. Phys. Chem. A*, 2008, **112**, 6630–6635.
- 22 H. B. Fu, X. Wang, H. B. Wu, Y. Yin and J. M. Chen, Heterogeneous uptake and oxidation of SO₂ on iron oxides, *J. Phys. Chem. C*, 2007, **111**, 6077–6085.
- 23 X. Zhao, L. Kong, Z. Sun, X. Ding, T. Cheng, X. Yang and J. Chen, The Interactions between Heterogeneous Uptake and Adsorption of Sulfur Dioxide and Acetaldehyde on Hematite, *J. Phys. Chem. A*, 2015, **119**, 4001–4008.
- 24 F. J. Dentener, G. R. Carmichael, Y. Zhang, J. Lelieveld and P. J. Crutzen, Role of mineral aerosol as a reactive surface in the global troposphere, *J. Geophys. Res.: Atmos.*, 1996, **101**, 22869–22889.
- 25 H. Guo, H. Xu and A. S. Barnard, Can hematite nanoparticles be an environmental indicator?, *Energy Environ. Sci.*, 2013, **6**, 561–569.
- 26 R. M. Cornell and U. Schwertmann, *The Iron Oxides*, WileyVCH, Weinheim, Germany, 2nd edn, 2003.
- 27 H. Guo and A. S. Barnard, Naturally occurring iron oxide nanoparticles: morphology, surface chemistry and environmental stability, *J. Mater. Chem. A*, 2013(1), 27–42.
- 28 A. S. Madden, V. E. Hamilton, M. E. E. Madden, P. R. Larson and M. A. Miller, Low-temperature mechanism for formation of coarse crystalline hematite through nanoparticle aggregation, *Earth Planet. Sci. Lett.*, 2010, **298**, 377–384.
- 29 A. S. Barnard and H. Guo, *Nature's Nanostructures*, Pan Stanford, 2012.
- 30 C. R. Usher, A. E. Michel and V. H. Grassian, Reactions on mineral dust, *Chem. Rev.*, 2003, **103**, 4883–4940.
- 31 W. Sun, Q. Meng, L. Jing, D. Liu and Y. Cao, Facile Synthesis of Surface-Modified Nanosized α -Fe₂O₃ as Efficient Visible Photocatalysts and Mechanism Insight, *J. Phys. Chem. C*, 2013, **117**, 1358–1365.
- 32 R. Suresh, K. Giribabu, R. Manigandan, A. Vijayaraj, R. Prabu, A. Stephen and V. Narayanan, α -Fe₂O₃ nanoflowers: synthesis, characterization, electrochemical sensing and photocatalytic property, *J. Iran. Chem. Soc.*, 2014, **11**, 645–652.
- 33 Q. Tong, T. Jiao, H. Guo, J. Zhou, Y. Wu, Q. Zhang and Q. Peng, Facile Synthesis of Highly Crystalline α -Fe₂O₃ Nanostructures with Different Shapes as Photocatalysts for Waste Dye Treatment, *Sci. Adv. Mater.*, 2016, **8**, 1005–1009.
- 34 G. Zhang, Y. Gao, Y. Zhang and Y. Guo, Fe₂O₃-pillared rectorite as an efficient and stable Fenton-like heterogeneous catalyst for photodegradation of organic contaminants, *Environ. Sci. Technol.*, 2010, **44**, 6384–6389.
- 35 X. S. Nguyen, G. Zhang and X. Yang, Mesocrystalline Zn-doped Fe₃O₄ hollow microspheres: formation mechanism and enhanced photo-Fenton catalytic performance, *ACS Appl. Mater. Interfaces*, 2017, **9**, 8900–8909.
- 36 C. Xiao, J. Li and G. Zhang, Synthesis of stable burger-like α -Fe₂O₃ catalysts: formation mechanism and excellent photo-Fenton catalytic performance, *J. Cleaner Prod.*, 2018, **180**, 550–559.
- 37 F. Yang, H. Chen, J. Du, X. Yang, S. Gao, J. Chen and F. Geng, Evolution of the mixing state of fine aerosols during haze events in Shanghai, *Atmos. Res.*, 2012, **104**, 193–201.

- 38 G. Zhang, X. Bi, L. Li, L. Chan, M. Li, X. Wang, G. Sheng, J. Fu and Z. Zhou, Mixing state of individual submicron carbon-containing particles during spring and fall seasons in urban Guangzhou, China: a case study, *Atmos. Chem. Phys.*, 2013, **13**, 4723–4735.
- 39 K. Adachi and P. R. Buseck, Changes in shape and composition of sea-salt particles upon aging in an urban atmosphere, *Atmos. Environ.*, 2015, **100**, 1–9.
- 40 L. Shao, J. Liu, X. Song, H. Niu and F. Zhang, Characteristics of Pollution and Microscopic Morphology of Atmospheric Particulate Matter in Beijing during 2008 Olympics and Paralympics, *Geosciences*, 2010, **2**, 337–344.
- 41 W. Li, L. Shao, D. Zhang, C.-U. Ro, M. Hu, X. Bi, H. Geng, A. Matsuki, H. Niu and J. Chen, A review of single aerosol particle studies in the atmosphere of East Asia: morphology, mixing state, source, and heterogeneous reactions, *J. Cleaner Prod.*, 2016, **112**, 1330–1349.
- 42 L. Wang, F. Zhang and J. Chen, Carbonyl sulfide derived from catalytic oxidation of carbon disulfide over atmospheric particles, *Environ. Sci. Technol.*, 2001, **35**, 2543–2547.
- 43 J. Liu, J. Wang, J. Sun and Y. Li, Hydrothermal synthesis and characterization of monodisperse α -Fe₂O₃ nanocubes, *Micro Nano Lett.*, 2014, **9**, 746–749.
- 44 C. Su and H. Wang, Capsule-like α -Fe₂O₃ nanoparticles: Synthesis, characterization, and growth mechanism, *Cryst. Res. Technol.*, 2012, **47**, 896–902.
- 45 S. Han, L. Hu, Z. Liang, S. Wageh, A. A. Al-Ghamdi, Y. Chen and X. Fang, One-step hydrothermal synthesis of 2D hexagonal nanoplates of α -Fe₂O₃/graphene composites with enhanced photocatalytic activity, *Adv. Funct. Mater.*, 2014, **24**, 5719–5727.
- 46 S. J. Hug, In situ Fourier transform infrared measurements of sulfate adsorption on hematite in aqueous solutions, *J. Colloid Interface Sci.*, 1997, **188**, 415–422.
- 47 L. Li, Z. M. Chen, Y. H. Zhang, T. Zhu, J. L. Li and J. Ding, Kinetics and mechanism of heterogeneous oxidation of sulfur dioxide by ozone on surface of calcium carbonate, *Atmos. Chem. Phys.*, 2006, **6**, 2453–2464.
- 48 C. E. Nanayakkara, J. Pettibone and V. H. Grassian, Sulfur dioxide adsorption and photooxidation on isotopically-labeled titanium dioxide nanoparticle surfaces: roles of surface hydroxyl groups and adsorbed water in the formation and stability of adsorbed sulfite and sulfate, *Phys. Chem. Chem. Phys.*, 2012, **14**, 6957–6966.
- 49 A. L. Goodman, P. Li, C. R. Usher and V. H. Grassian, Heterogeneous uptake of sulfur dioxide on aluminum and magnesium oxide particles, *J. Phys. Chem. A*, 2001, **105**, 6109–6120.
- 50 A. Preszler Prince, P. D. Kleiber, V. H. Grassian and M. A. Young, Heterogeneous interactions of calcite aerosol with sulfur dioxide and sulfur dioxide/nitric acid mixtures, *Phys. Chem. Chem. Phys.*, 2007, **9**, 3432–3439.
- 51 G. Pacchioni, A. Clotet and J. M. Ricart, A Theoretical-Study of the Adsorption and Reaction of SO₂ at Surface and Step Sites of the MgO(100) Surface, *Surf. Sci.*, 1994, **315**, 337–350.
- 52 T. Wang, Y. Liu, Y. Deng, H. Fu, L. Zhang and J. Chen, Emerging investigator series: heterogeneous reactions of sulfur dioxide on mineral dust nanoparticles: from single component to mixed components, *Environ. Sci.: Nano*, 2018, **5**, 1821–1833.
- 53 J. Baltrusaitis, D. M. Cwiertny and V. H. Grassian, Adsorption of sulfur dioxide on hematite and goethite particle surfaces, *Phys. Chem. Chem. Phys.*, 2007, **9**, 5542–5554.
- 54 T. Wang, Y. Liu, Y. Deng, H. Fu, L. Zhang and J. Chen, The influence of temperature on the heterogeneous uptake of SO₂ on hematite particles, *Sci. Total Environ.*, 2018, **644**, 1493–1502.
- 55 J. Park, M. Jang and Z. Yu, Heterogeneous Photooxidation of SO₂ in the Presence of Two Different Mineral Dust Particles: Gobi and Arizona Dust, *Environ. Sci. Technol.*, 2017, **51**, 58617–58627.
- 56 P. D. Wade, J. Taylor and P. Siekevitz, Mammalian cerebral cortical tissue responds to low-intensity visible light, *Proc. Natl. Acad. Sci. U. S. A.*, 1988, **85**, 9322–9326.
- 57 A. Kojima, K. Teshima, Y. Shirai and T. Miyasaka, Organometal halide perovskites as visible-light sensitizers for photovoltaic cells, *J. Am. Chem. Soc.*, 2009, **131**, 6050–6051.
- 58 B. C. Faust, M. R. Hoffmann and D. W. Bahnemann, Photocatalytic oxidation of sulfur dioxide in aqueous suspensions of α -iron oxide (Fe₂O₃), *J. Phys. Chem.*, 1989, **93**, 6371–6381.
- 59 M. Mishra and D. M. Chun, α -Fe₂O₃ as a photocatalytic material: A review, *Appl. Catal., A*, 2015, **498**, 126–141.